Journal of Power Sources 472 (2020) 228614

Contents lists available at ScienceDirect

Journal of Power Sources

journal homepage: www.elsevier.com/locate/jpowsour

18650 vs. 21700 Li-ion cells – A direct comparison of electrochemical, thermal, and geometrical properties

Thomas Waldmann *, Rares-George Scurtu, Karsten Richter, Margret Wohlfahrt-Mehrens

ZSW – Zentrum für Sonnenenergie- und Wasserstoff-Forschung, Baden-Württemberg, Helmholtzstrasse 8, D-89081, Ulm, Germany

HIGHLIGHTS

- Direct comparison of 18650 and 21700 formats with same chemistry.
- Comparison of electrochemical, thermal, and geometrical properties.
- Similarity in voltage curves and ageing at 1C/25 °C.
- Internal temperature sensors show stronger heating of 21700 format.
- New method for analysis of jelly rolls via digitalization of CT images.

GRAPHICAL ABSTRACT

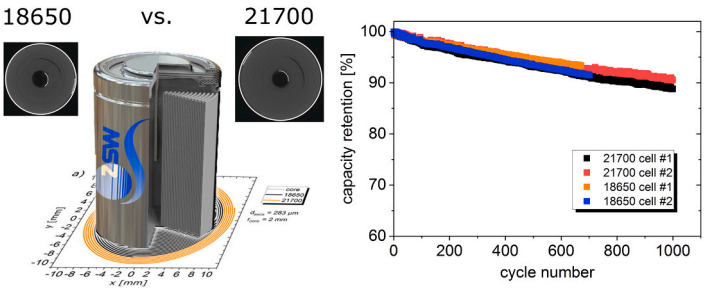

ARTICLE INFO

Keywords:
Lithium-ion cells
21700
18650
Cell format
Electrode curvature
Archimedean spiral

ABSTRACT

Li-ion cells of the classic 18650 format are directly compared with the new 21700 format regarding electrochemical, thermal, and geometrical properties. Both types of cells were reproducibly built on pilot scale with the same electrodes, separator, and electrolyte allowing a direct comparison for the first time. Internal temperature sensors give insights on the heating behaviour. Similarities are found in the voltage curves and capacity fade at 1C cycling at 25 °C. The capacity and energy increase per cell is ~50% from 18650 to 21700 for discharge in the range of 0.5C–3.75C. The results are compared with calculations of electrode areas based on Archimedean spiral's arc lengths and geometrical data extracted from X-ray computed tomography (CT) measurements. Two evaluation methods for extraction of the number of electrode windings from CT images are compared. Calculations are made for the winding number as a function of the periodic winding distance (thicknesses of anode, cathode, and 2x separator) as well as on electrode curvature for both cell formats. The influences of intended extensions of the cell diameter by few μm (as observed in commercial cylindrical cells), as well as larger formats such as 30700 on additional electrode windings and cell capacity are estimated.

1. Introduction

Wound electrodes have the advantage of faster production compared to stacked electrodes. Since its market introduction in 1994, the 18650 format became a popular standard for Li-ion cells across the consumer industry. Increases in diameter by 3 mm and in height by 5 mm lead to the new 21700 format. Similarly for both cell formats is the wound jelly roll which has approximately the form of an Archimedean spiral [1–5].

Although there is a variety of papers on the classic 18650 format [6–11], literature on the new 21700 format is still very scarce [7,11,12].

* Corresponding author.
E-mail address: thomas.waldmann@zsw-bw.de (T. Waldmann).

https://doi.org/10.1016/j.jpowsour.2020.228614
Received 15 May 2020; Received in revised form 9 June 2020; Accepted 2 July 2020
Available online 20 July 2020

By evaluation of commercial cells, we have recently shown that the changes from 18650 to 21700 result in ~50% more energy content per cell for 0.5C discharging [7]. This has the potential to reduce production costs, since 33% fewer cells have to be produced for a similar energy content [7]. However, since the subject of our previous study were commercial cells with variations in chemistry, electrode types, and details in cell design, a direct comparison is still missing. For example, differences in the charge and discharge voltage curves or ageing of both cell formats could only be compared when the used electrochemically relevant cell components are the same.

Regarding cell design there is a number of simulation studies, mostly on the effect of tab design [1,2,13–18]. For example, McCleary et al. calculated the temperature distribution along the electrodes for different tab numbers [2]. To best of our knowledge, there are currently no experimental results available which are directly comparing the classic 18650 and the new 21700 format. However, such a direct comparison is highly needed to gain further insights into the differences and similarities of both cell formats.

Therefore, in the present paper we built 18650 and 21700 Li-ion cells with the same electrodes, separator, and electrolyte. These cells directly show differences and similarities induced by the cell format change only. Additionally, the cells are equipped with internal temperature sensors to reveal trends in temperature differences. The measurements are complemented by calculations of Archimedean spiral arc lengths, electrode areas, capacities, and electrode curvatures to reveal further details on both cell formats.

2. Experimental

2.1. Materials

18650 and 21700 type cells were built at ZSW's pilot-line [19,20]. The properties of the electrodes are summarized in Table 1. We would like to mention that the built 18650 and 21700 cells are not optimized regarding neither high energy nor high power. However, they are well suited for a direct comparison with the same chemistry which was the main intention of the present paper. Therefore, for other chemistries, the observed trends will most likely be the same. For both cell formats the contents of electrolyte (~12 wt.-%), separator (~15 wt.-%) are very similar. The main differences are in weight of the electrodes (18650: 53 wt.-%, 21700: 55 wt.-%) and housing (18650: 20 wt.-%, 21700: 18 wt.-%).

The electrolyte amounts (1 M $LiPF_6$ in EC : EMC = 3 : 7 (wt.-%) + 2% VC) were 5 mL and 7 mL in the 18650 and 21700 cells, respectively. Celgard H1609 was used as separator. The housing materials and wall thicknesses are the same for both formats (0.3 mm). One difference is in the positive terminal which has a higher resistance for the 18650 cell.

Type K thermocouples were placed in a dry room (dew point < −65 °C) in the cylindrical empty space at mid-height of the jelly roll and on the cell surface. In both cases, the tips of the sensors were positioned at distances of 30.8 mm and 32.8 mm from the bottom of the 18650 and 21700 cans, respectively. The temperatures were recorded operando by a data logger (Hioki Memory HiLogger LR8400).

Table 1
Overview on properties of the electrodes and separator built into 18650 and 21700 cells.

	Anode	Cathode
Active material	graphite	$Li_xNi_{0.33}Mn_{0.33}Co_{0.33}O_2$
Electrode thicknesses (double side coated)	126 µm	125 µm
Current collector foil thicknesses	10 µm (Cu)	20 µm (Al)
Areal capacity	5.00 mAh/cm^2	4.12 mAh/cm^2
N/P ratio		1.21
Separator thickness		16 µm

2.2. Electrochemical tests

All electrochemical tests were conducted by a Basytec XCTS (max. 25A) cycler in a Vötsch climate chamber with 20 °C and 25 °C ambient temperature for charging and discharging, respectively. We note that the different temperatures for charging and discharging originate from the history of cell testing in our lab. The accuracies of the temperature chamber, voltage, and current are ±0.2 °C, ±5 mV, and ±1 mA, respectively.

The cells were formatted by 3 cycles (0.1C CC-CV, CV until 0.05C) in the voltage range of 2.8–4.2 V. The C-rates in the discharge (CC) tests were 0.5C, 1C, 1.5C, 2C, 2.5C, 3C, 3.5C, and 3.75C. The charging C-rate in discharge rate capability tests was fixed to 0.5C in the CC phase, the CV phase was stopped when I < 0.1C. The C-rates in the charge (CC) tests were 0.1C, 0.5C, 1C, 2C, and 3C. In these tests, the discharging (CC) C-rate was fixed to 0.5C. After charging a 4 h and after discharging a 0.5 h rest period were applied to ensure a constant OCV period. Discharging rate capability tests were carried out before charging rate-capability tests in order to exclude effects of possible Li deposition. On detailed overview on cells, tests, and evaluation methods is given in Table 2.

2.3. Quality of cells and reproducibility

Mean values and standard deviations for cell capacity, mass, and internal resistance were 1.625 ± 0.007 Ah, 40.99 ± 0.03 g, and 25.0 ± 0.2 mΩ for the 18650 cells and 2.457 ± 0.040 Ah, 59.71 ± 0.10 g, and 13.2 ± 0.1 mΩ for the 21700 cells, respectively. The basis of this evaluation are four 18650 cells and three 21700 cells. The values for capacity, mass, and internal resistance were very similar. To describe this similarity we used mean values and standard deviations implemented in Excel 2016.

Cell resistances were measured at a frequency of 1 kHz using the resistance meter Hioki RM3548 with 0.02% basic accuracy. These values are in a similar range like for mass produced cylindrical cells [7]. Furthermore, the voltage curves in Fig. 1 show a high degree of reproducibility for both 18650 and 21700 cells for individual discharge C-rates. A comparison of both formats is achieved by normalizing the capacity of both formats, i.e. 100% corresponds to a full discharge and charge at the lowest C-rate, in Fig. 1 a and b, respectively. In Fig. 1, the data of two cells of each format are plotted (no mean values). The reproducibility is visible in the coincidence of the superimposed curves.

X-ray computed tomography (CT) scans (v|tome|x 300) show that the electrodes in the jelly rolls of both formats are well aligned. Therefore, the pilot-line made cells are suitable for further tests. All tests were reproduced with at least one additional cell.

Cell diameters of commercial cells were measured for three cells at five positions each to exclude deviations between the cells as well as effects from deviations from perfect circular shape. The exemplarily given value in the text represents the mean value and the standard deviation from these measurements.

3. Results and discussion

3.1. Direct electrochemical and thermal comparison of 18650 and 21700 cells

Fig. 1a shows that the voltage curves plotted vs. normalized discharge capacity are similar for both formats in the range of 0.5C–3.75C. For 0.5C, the voltage curves of both formats coincide. However, the difference in polarization between both formats increases slightly with higher C-rates. This could be explained on one hand due to the lower resistance of the 21700 cell (R_{18650} = 25.0 ± 0.2 mΩ, R_{21700} = 13.2 ± 0.1 mΩ) and on the other hand due to the tendency of higher temperatures inside the jelly roll and on the cell surface of the 21700 cell (see Fig. 2c). Similarly to the discharge curves, also the charging curves are very similar for 18650 and 21700 in the range of 0.1C–3C, with a

Table 2
Overview on cells investigated in this study and evaluation methods. *Mean value and standard deviation calculated by Excel 2016, ** Linear fits in Origin 2019b.

Cell	Origin	Test	Data evaluation	
18650_cell1	pilot line	1) Discharge rate capability	1a) Discharge capacity and energy: Mean value and standard deviation* of cells 1–3 (Fig. 2a and b)	Capacity and energy ratios 21700:18650 (Fig. 2a and b)
18650_cell2	pilot line	2) Charging rate capability		
18650_cell3	pilot line		1b) Mean value and standard deviation of maximum internal temperatures of cells 1–3 (Fig. 2c)	Mean value* of 18650's and 21700's mean capacities and energies from (1a)
			2) Individual voltage curves for cells 1 & 2 (Fig. 1)	Error estimated from maximum standard deviation of 18650 and 21700 cells from (1a)
21700_cell1	pilot line	1) Discharge rate capability	1a) Discharge capacity and energy: Mean value and standard deviation* of cells 1–3 (Fig. 2a and b)	
21700_cell2	pilot line	2) Charging rate capability		
21700_cell3	pilot line		1b) Mean value and standard deviation of maximum internal temperatures of cells 1–3 (Fig. 2c)	
			2) Individual voltage curves for cells 1 & 2 (Fig. 1)	
18650_cell4	pilot line	Cycling at 1C/25 °C	Individual fits of lines in Fig. 8 with slope and error of slope** for each cell	Mean value* of slopes from two cells of each format. The maximum slope error was rounded up
18650_cell5	pilot line			
21700_cell4	pilot line			
21700_cell5	pilot line			
21700_cell6	commercial	Measurement of cell diameters at mid-height	Mean value* and standard deviation* of five measurements for cells 6-8	
21700_cell7	commercial			
21700_cell8	commercial			

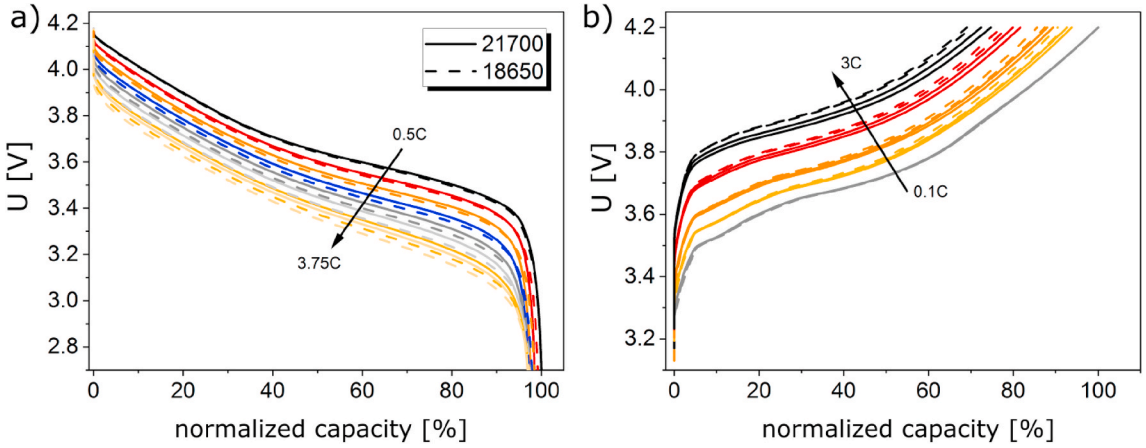

Fig. 1. Direct comparison of voltage curves of 18650 (dashed lines) and 21700 cells (solid lines). a) Discharge curves for an ambient temperature of 25 °C (black: 0.5C, red: 1C, orange: 1.5C, blue: 2C, dark grey: 2.5C, light grey: 3C, dark yellow: 3.5C, light yellow: 3.75C) and b) charging curves for an ambient temperature of 20 °C (dark grey: 0.1C, yellow: 0.5C, orange: 1C, red: 2C, black: 3C). Arrows indicate increasing C-rates. (For interpretation of the references to colour in this figure legend, the reader is referred to the Web version of this article.)

tendency of stronger polarization in case of higher C-rates (Fig. 1b). In contrast, Lain et al. recently showed voltage curves of commercial 18650 and 21700 cell, both from Samsung with a graphite + Si/NCA chemistry [11]. Although the SEM images of anode and cathode looked very similar, the voltage curves did not coincide [11]. Comparing the discharge energies of both commercial cell types yields an increase by a factor of 1.58 [11], therefore the materials might be similar, however most likely not the areal capacities of the electrodes. In contrast, the chemistry and electrode loading are the same in our experiment, leading to the observed coincidence of the voltage curves in Fig. 1.

We would like to note that the standard deviations of the external and internal cell temperatures in Fig. 2c are overlapping and therefore we cannot conclude on absolute differences between 18650 vs. 21700 in the present study. We expect that the differences in heating behaviour (between 18650 and 21700 as well as mean radial temperature gradients) are most likely more pronounced for thicker electrodes [21]. Nevertheless, the temperature data indicate three trends: i) Higher internal maximum temperatures during discharging were observed for increasing C-rates. This is consistent with results on temperatures on the cell surface by Grandjean et al. for 20 Ah pouch cells [22], with our previous paper on different types of 18650 cells [21], and with our previous study on internal cell temperatures for 18650 cells [23]. ii) Stronger mean radial temperature gradients from inside the jelly roll to the cell surface with increasing cell radius, i.e. from 18650 to 21700. iii) A tendency of stronger heating for the larger 21700 format is indicated in the present paper. This trend is consistent with our previous study with external temperature sensors on commercial 18650 and 21700 cells [7]. Additionally, this trend is consistent with the heating behaviour of a graphite anode and NCA cathode reconstructed from commercial 3.25 Ah 18650 cells into small lab pouch cells (~0.1 Ah), which showed no temperature increase on the cell surface in contrast to the original 18650 cells [24]. In that case, a stronger polarization had been observed for the smaller pouch cells which have – in similarity to the present study – a lower mean temperature at the end of discharge and a higher resistance [24].

We note that the maximum mean radial temperature difference in both, 18650 and 21700 cells, scales mostly linearly with the discharge C-rate for a full discharge. This is consistent with temperature differences on the surface of 50 Ah pouch cells by Veth et al. [25] and with data on radial temperature differences in commercial 18650 cells [23].

Fig. 2 shows the discharge capacities, discharge energies and their ratios for the cell formats 21700 : 18650 as a function of discharge C-rate. Fig. 2a shows that the discharge capacities for 18650 and 21700 cells are stable for discharge rates in the range of 0.5C–3.75C. It is noted that the error bars (representing standard deviations of measurements with three cells) for the capacities are comparably small, indicating a very good reproducibility for the cells for each of the two formats. A similar discharge rate capability was observed for commercial

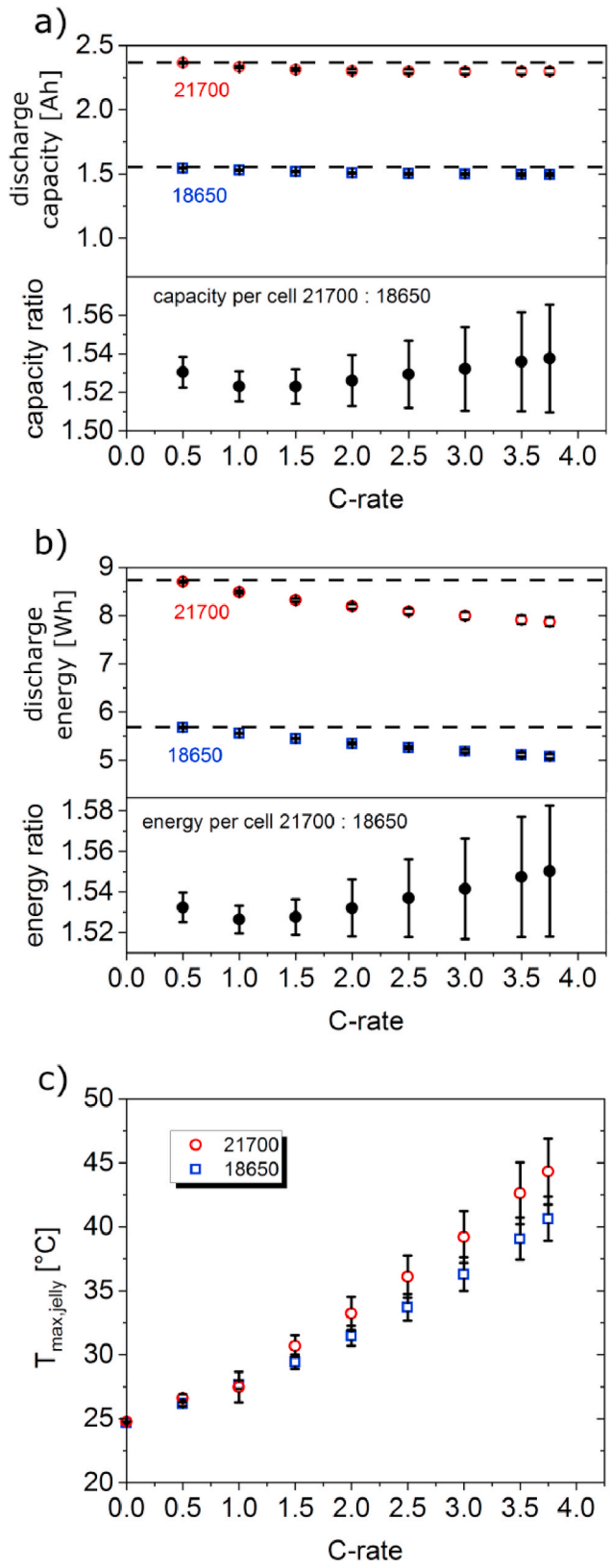

Fig. 2. a) Discharge capacity and b) discharge energy at an ambient temperature of 25 °C with respective ratios for the 21700 : 18650 formats as a function of discharge C-rate. The dashed lines display values at 0.5C and are intended to show the deviation at higher C-rates. c) Maximum temperatures inside the jelly roll for 18650 and 21700 cells (mean temperatures and standard deviations from three cells each).

cylindrical cells [7]. The stable discharge C-rate capability regarding capacity is likely to originate from stronger temperature rises at higher C-rates [21–23].

The different heating behaviour influences the diffusion kinetics of Li in graphite and can therefore explain the observed differences in polarization. The ratio of diffusivities in the core of 21700 to 18650 cells can be estimated (see eq. (3) in Ref. [26]). For discharging at 3.5C ($\Delta T \approx$ 2.7 °C between 18650 and 21700 in cell core), this estimation yields a maximum ratio of the diffusivities for 21700 vs. 18650 of 1.10 in case of Li diffusion in $Li_{0.2}C_6$ (barrier = 0.308eV [27]). In case of a similar heating behaviour during charging, it is likely that 21700 cells show a lower susceptibility to Li deposition compared to 18650 cells for the same cell chemistry and electrodes.

As shown in the lower part of Fig. 2a, the capacity ratios (21700 : 18650) are in the range of 1.53 ± 0.01 for discharging at 0.5C at an ambient temperature of 20 °C. This is in good agreement with our previous evaluation of energy ratios of commercial cells based on typical cylinder volumes (~1.49) and from typical diameters of 18650 compared with X-ray CT measurements of a 21700 cell (~1.49) [7]. For higher discharge C-rates, the capacity ratio remains in the same range, however, the error bar gets larger, e.g. 1.53 ± 0.03 for discharge at 3.75C. This is consistent with the ratio of 1.52 of the cathode areas (767.2 cm^2 for 18650 and 1164.0 cm^2 for 21700).

Fig. 2b shows the discharge energies for 18650 and 21700 cells. In contrast to the discharge capacities, the discharge energies show a tendency of decrease with higher C-rate. The reason is the stronger heating for higher C-rates (compare Fig. 2c). Therefore, more electrochemical energy is converted into thermal energy instead of electrical energy at higher C-rates.

The energy ratios (21700 : 18650) are in the same range as the capacity ratios. For 0.5C, this is in agreement with our previous study on different commercial cells, which had allowed only an indirect comparison [7]. The results from the present study furthermore substantiate our recent estimation on production efforts per Wh for 21700 cells compared to 18650 cells [7].

Comparison of the discharge energies furthermore allows for a comparison of the specific energies. According to the direct comparison in the present paper, the specific energy increases by ~6% when changing the format from 18650 to 21700. In our previous estimation based on cylinder volumes, the increase of specific energy was ~2% [7], which is in the same order of magnitude. However, the increase to ~6% shows that e.g. the positive terminal might leave some room for further optimization in specific energy.

3.2. *Direct geometrical comparison*

Fig. 3 shows a direct comparison of the 18650 and 21700 cells via X-ray computed tomography (CT) measurements. Fig. 3b,e correspond to 2D cross-sections at mid-height of the cylinders (see inset in Fig. 3a). Heavier elements or regions with higher density show a higher X-ray absorption and are therefore displayed brighter (higher grey scale value) [4]. Therefore, the housing (mostly Fe), the tabs (Al, Ni), the jelly roll (Ni, Mn, Co, Al, Cu, C, Li), as well as the gas filled core of the jelly roll (displayed dark) can be distinguished.

Line scans along the dashed lines in the 2D cross-sections are depicted in Fig. 3a,d. The periodicity in the grey scale values of the line scans represent anode and cathode and therefore allow counting the windings. The approximate number of windings can be extracted from the peak number in the line profiles [7]. 42 and 52 peaks correspond to 21 and 26 windings of the jelly roll for the 18650 and the 21700 cell, respectively. Please note that the method using line scans does not take the exact start and end angle of the jelly roll into account, however, it can be used for a quick estimation.

A more exact method to measure the number of windings is 'digitizing' the windings. The windings in the CT cross-section (e.g. Fig. 3b) are superimposed with a line. This spiral-like line (e.g. Fig. 3c)

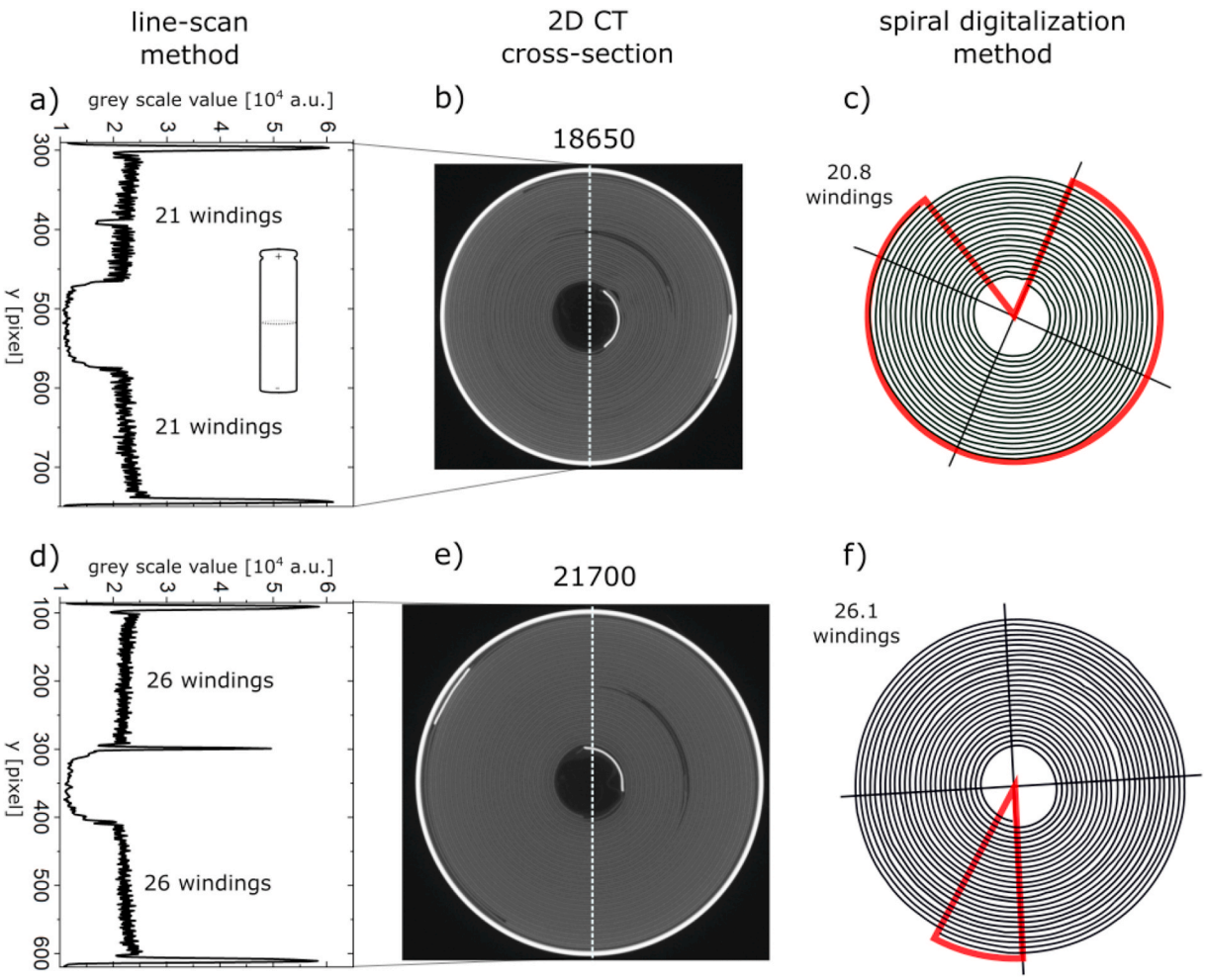

Fig. 3. Evaluation of CT cross-sections of a)-c) 18650 and d)-f) 21700 cell. b) and e) 2D cross-sections of CT data at mid-height of the cylinders (see inset in (a)). a) and d) line profiles along the dashed lines in b) and e), respectively. c) and f) digitalization of spiral in b) and e), respectively.

represents the 'digitized' windings of the cross-section and can be used to obtain the winding number and electrode length. For the 18650 and 21700 cell, the number of windings obtained by this method are 20.8 and 26.1, respectively.

For further comparison, the Archimedean spiral curve can be modelled in polar coordinates according to Ref. [2,5] by

$$r = a \cdot \phi \tag{1}$$

where r is the radius defining the spiral line and the ϕ the polar angle. The factor a is related via

$$a = \frac{d_{ascs}}{2\pi} \tag{2}$$

to the periodic distance between the windings d_{ascs} in the jelly roll. For a cylindrical cell, d_{ascs} corresponds to the sum of the thicknesses of anode, cathode (both double side coated), and two times the thickness of the separator (see Fig. 4b). We had previously introduced d_{ascs} (called d in Ref. [21]) and reported that it has an influence on cell resistance and heating behaviour of 18650 cells [21]. I.e. in 18650 cells, higher d_{ascs} values lead to higher maximum temperatures during full discharge as a function of C-rate [21]. On the other hand, for fixed cell radii, higher d_{ascs} values lead to increased cell resistances, since the electrochemically active cathode area is decreased due to less electrode windings [7,21].

Fig. 4a represents an Archimedean spiral constructed from eq. (1) for a value of d_{ascs} = 283 μm corresponding to the experimental cells in Fig. 3 (see Table 1 for calculation of d_{ascs} value). The 'core windings' (not present in the cell), windings of the 18650 format and additional windings of the 21700 format are depicted in grey, black, and orange, respectively.

It has to be noted that real cylindrical cells show deviations from the mathematically perfect form given by eq. (1) (compare Fig. 3b,e and Fig. 4a) [4,28–31]. The main deviations for fresh cells originate from current collecting tabs, uncoated electrode parts, and deviations of the cell housing from a perfect cylinder. For cycling aged cells, even stronger deformations for the jelly roll were reported [4,28,30,31].

For further comparison of the 18650 and 21700 formats, the electrode areas have to be calculated. The arc length l of the Archimedean spiral is given by Ref. [2,5], and can be used to estimate the length of the additional windings in 21700 cells compared with 18650 cells. A longer arc length corresponds to longer cathodes and therefore increases the cell capacity and energy. We note that a factor h must be considered as well in order to account for the larger electrode width in case of the 21700 format (in the present study h = 1.08). The ratio of cell capacities for the 21700 and 18650 formats can then be calculated by the ratios of l from eq. (3) multiplied by h. Eq. (3) yields a difference of 5.3 windings between 18650 and 21700 cells if the corresponding value for the experimental cells of d_{ascs} = 283 μm is used. From the line scans of CT cross-sections in Fig. 3a,d, five additional windings were roughly estimated for the 21700 cell. The more exact (and more time consuming) method of digitizing the spiral from CT images in Fig. 3c,f yields 5.26 additional windings. Therefore, although the form of real jelly roll deviates to a small amount from the perfect Archimedean spiral generated

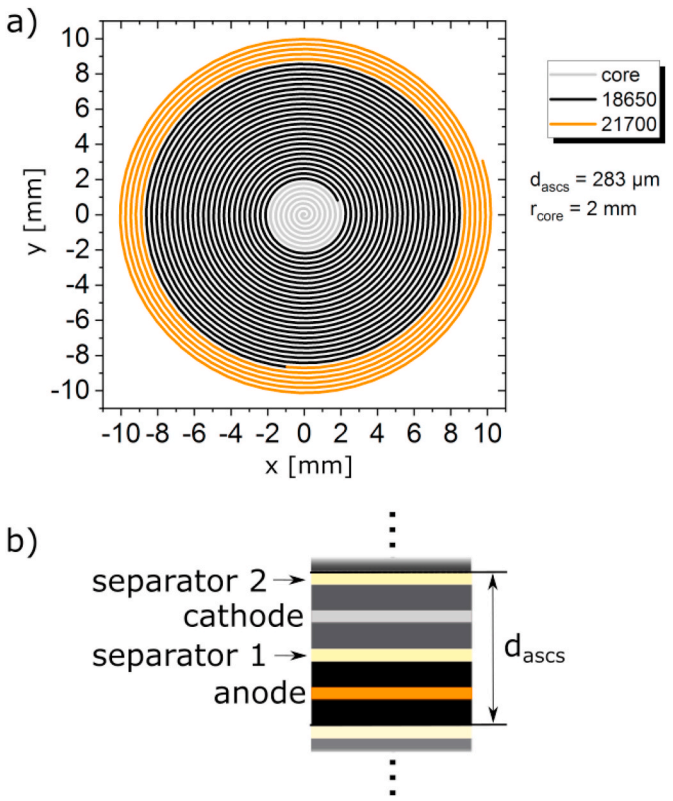

Fig. 4. a) Calculated Archimedean spiral according to eq. 1. b) Illustration of periodic winding distance d_{ascs} in jelly rolls of cylindrical cells.

by eq. (1), the number of additional windings is in very good agreement with the experiment and the spiral digitalization method.

$$l = \frac{a}{2}\left[\phi\sqrt{1+\phi^2} + \ln\left(\phi + \sqrt{1+\phi^2}\right)\right] \quad (3)$$

According to eq. (2) and taking into account the electrode width factor h, these additional windings at the outer part of the jelly roll for the 21700 cell correspond to 51% more energy for this cell format. Further evaluation of eq. (3) shows that the capacity ratio between the 21700 and the 18650 format is largely independent from d_{ascs}. This independency can be shown for the typical d_{ascs} values in the range of 200 µm–500 µm. This is accordance with the experimental results in Fig. 2, as well as with our previous study on commercial cylindrical cells [7].

Fig. 5 depicts the number of windings in the 18650 and 21700 formats (both without 'core windings') as a function of the periodic winding distance d_{ascs}. As expected, the number of windings in both the 18650 and the 21700 format decrease with increasing thicknesses of anode, cathode, and separator, and therefore d_{ascs}. It is interesting to see that the number of additional windings in the 21700 cells compared to 18650 are in the range of ~8 to ~3 for the wide range of 200 µm–500 µm for d_{ascs}, respectively. It must be noted that the higher areal capacities for higher d_{ascs} values compensate the less additional windings and therefore lead to the constant capacity ratio of ~1.5 (see above).

By multiplying the cathode area with the respective areal capacities, the winding numbers of the jelly roll can be translated into cell capacities. We note that the cathode is chosen since its area is usually smaller than the anode area, and therefore limits the cell capacity. As examples we used the values given by Yang and Wang for areal capacities and thicknesses for high-energy and high-power electrodes (graphite and NMC622 ($Li_xNi_{0.6}Mn_{0.2}Co_{0.2}O_2$)) [32]. We note that these types of electrodes vary not only in thickness, for example the high-power electrodes have a higher porosity and N/P ratio [32]. To calculate

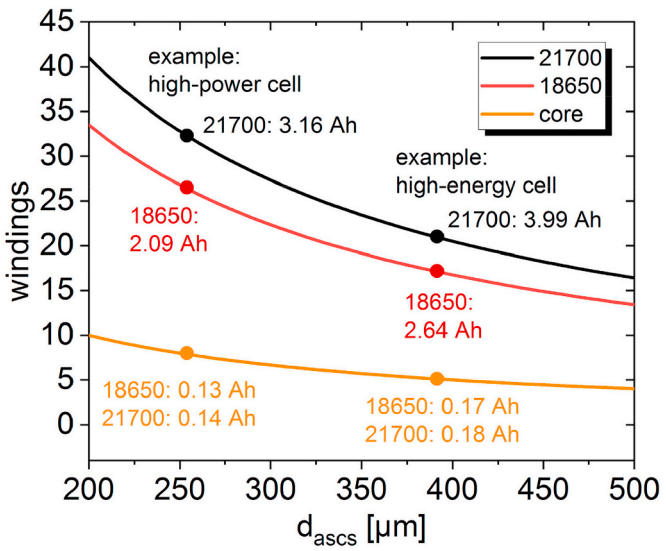

Fig. 5. Calculated number of windings in the jelly roll of 18650 and 21700 cells (both without core windings) as well as the theoretical (non-existing) core windings as a function of d_{ascs} for a core diameter of 2 mm. The two given examples, based on values from Ref. [32] for graphite/NMC622, show cell capacities for high-power and high-energy 18650 and 21700 cells (with without core windings) as well as the 'lost capacity' from non-existing core windings.

d_{ascs} we assumed typical thicknesses [12] of 10 µm, 15 µm, and 16 µm for the Cu and Al current collectors and the separator, respectively.

It can be seen from Fig. 5, that the thicker electrode coatings overcompensate the lower number of windings in the high-energy cells. The reason is the more favorable ratio of electrochemically active and inactive materials.

Furthermore, the non-existing 'virtual' windings of the core would correspond to only a minor amount of capacity (0.13–0.18 Ah). We note that the theoretical capacity of these inner windings is higher for the 21700 format due to the increased electrode width.

3.3. *Effects of cell housing dimensions*

When investigating commercial cylindrical cells, we found that the mean diameter at mid-height of the cylinders can exceed the expected value of 21.0 mm for the 21700 format. E.g. for a specific type of high-energy cells the diameter was 21.15 ± 0.02 mm. Maximum deviations in a similar range can be obtained from datasheets of commercial 18650 cells [33]. Although these could be seen as maximum manufacturing tolerances, it is likely that such diameter extensions are used in high-energy type cylindrical cells to gain additional electrode windings and therefore an increase of energy per cell. Indeed, when we had earlier constructed a heat sink for 18650 cells with a cylindrical hole of 18.0 mm in diameter [21], we had also observed that high-power cells often fitted into this device, whereas high-energy type cells often did not fit.

Fig. 6a depicts the number additional windings in the jelly roll of 21700 cell with additional diameters in the range of 50–400 µm. The number of additional windings is increasing stronger for thinner electrodes (lower d_{ascs} values) and with higher cell diameters. A maximum of one additional winding is possible for an additional 400 µm in cell diameter for a low value of d_{ascs} = 200 µm, corresponding to a high-power design.

Based on an estimation based on the data from Ref. [32], the gain in energy per cell by cell diameter increase is in the range of tens of mAh.

Fig. 6b shows the additional windings for cell formats with higher diameters in comparison to the 18650 format. E.g. for d_{ascs} = 200 µm, the known 20700 and 21700 formats have 5 and 7.5 more windings compared to the 18650 format, respectively. Based on the estimation by

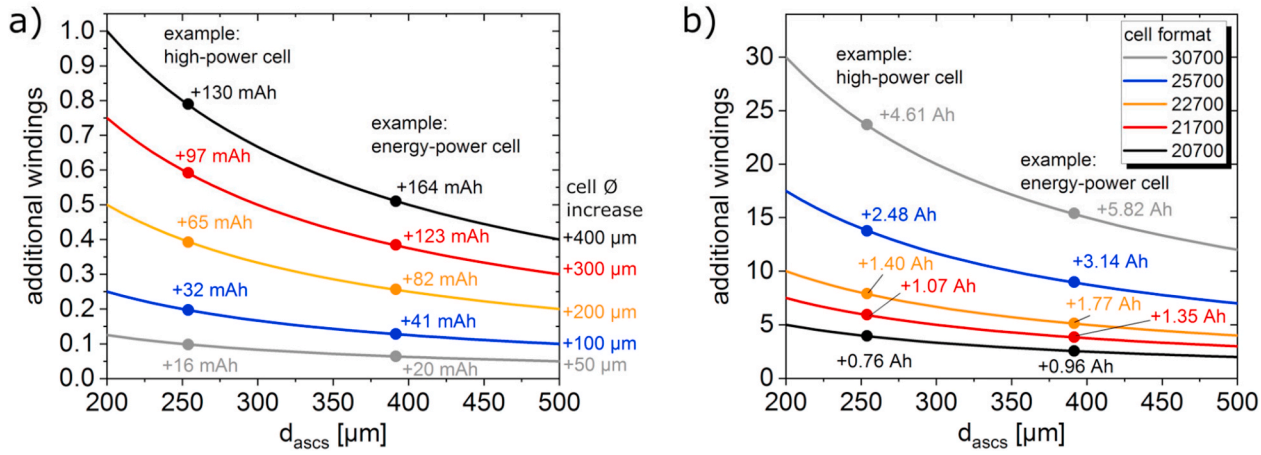

Fig. 6. Calculated additional windings for higher cell diameters. a) Additional windings for the 21700 format when increasing the cell diameter (compared to 21700 with 21.00 mm diameter). b) Additional windings in the formats 20700 to 30700 compared to the 18650 format as a function of d_{ascs}. The capacity values are examples based on values from Ref. [32] for high-power and high energy cells with graphite/NMC622.

data from Ref. [32], this leads to a capacity gain for high-energy cells of 0.96 Ah and 1.35 Ah per cell for 20700 and 21700 in comparison with 18650, respectively.

Further extrapolation to cell formats like 22700, 25700, and 30700 formats leads to a capacity gain per high-energy cell of 1.77 Ah, 3.14 Ah, and 5.82 Ah, respectively, compared to the 18650 format. It is noted that the increasing cell size leads to an increase of energy density, due to a better ratio of energy storing vs. non-energy storing volumes.

3.4. Effects of electrode curvature in 18650 and 21700 cells

The curvature of different windings in the jelly roll is also an important factor in the development of cylindrical Li-ion cells as well as for cells with wound jelly roll in general. The curvature κ of an Archimedean spiral given by Ref. [5]

$$\kappa = \frac{\phi^2 + 2}{a(\phi^2 + 1)^{\frac{3}{2}}} \tag{4}$$

which is dependent on the polar angle (and therefore the winding number) and to the periodic winding distance d_{ascs} via eq. (2). It is noted that the curvature for a certain winding can also be estimated by the curvature r^{-1} of a respective circle with radius r.

Fig. 7a shows the curvature for three cases of d_{ascs} as a function of winding number (higher winding number on outside of jelly roll) according to eq. (4). The curvature of the electrodes is higher i) for lower values of d_{ascs}, i.e. thinner electrodes and ii) for the inner windings in the jelly roll.

The comparably high curvatures in the inner windings (0.5 to 5 mm^{-1}) are avoided since this part is usually not filled with electrodes, i.e. empty [4,30,34] or supported with a mandrel [4,29,31,34–36]. Assuming similar core radii of 2 mm for the 18650 and the 21700 format, the curvatures of the first inner winding of the jelly rolls are very similar in both cases. For the outer windings, the curvature is also in a similar range for different electrode thicknesses and similar for 18650 and 21700 cells (see inset of Fig. 7a).

The electrode curvature and coating thickness are likely to induce differences in the electrode coatings which are facing towards the cell core (concave) and towards the cell housing (convex), i.e. the electrode coating facing towards the cell housing gets decompressed while the

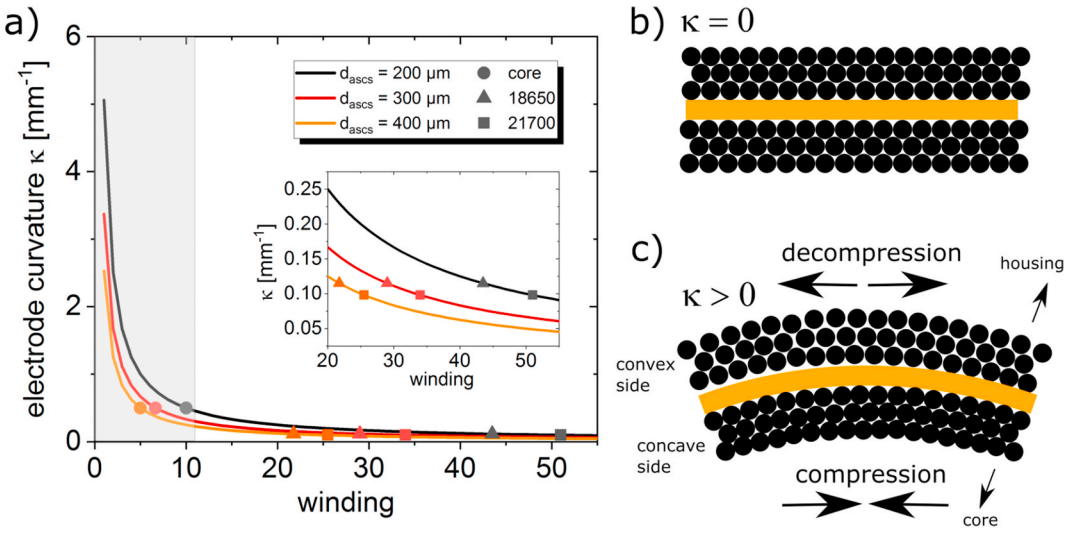

Fig. 7. a) Calculated electrode curvatures for cylindrical cells. The shaded area on the left indicates typical winding numbers in the core of the jelly roll. The inset shows an enlargement of the outer windings. Circles, triangles, and squares mark the end of cell core, as well as the outer windings of 18650 and 21700 cells, respectively. Please note that the windings for 18650 and 21700 cells are including the virtual core windings in (a). b) Illustration of a flat in comparison to c) a bended double side coated electrode. The convex side and concave sides are facing towards the cell housing and cell core, respectively.

electrode coating facing towards the cell core gets compressed (Fig. 7c). This results most likely in compressive mechanical stress and lower porosity for the electrode coating facing towards the cell core and the other way round for the electrode coating facing towards the cell housing.

Indeed, we have observed differences in the adhesion of the in anode coating in post-mortem analysis for different types of commercial cylindrical cells. The adhesion loss of anode coatings, especially in aged cells is often stronger for thicker electrode coatings, the inner windings near the core of the jelly roll, and for the coatings facing toward the cell core. This is consistent with the estimation by eq. (4) and with the model in Fig. 7c. Due to the similarity of the respective curvatures in the inner and outer parts of the jelly roll in Fig. 7a, this effect can be expected to be also similar for both formats.

From the results above, a similar effect can be expected in the curved parts of flat-wound jelly rolls ($\kappa > 0$, Fig. 7c), e.g. in pouch or prismatic cells. This effect for curved electrodes is in contrast to flat electrodes with no curvature ($\kappa = 0$, Fig. 7b), e.g. in stacked pouch cells or in the flat parts of flat-wound jelly rolls. In agreement with this, Mussa et al. found differences in the local cathode impedance between the curved outer and inner regions of the coating in prismatic cells with a flat wound jelly roll [37]. In contrast, the impedance between outer and inner part of the flat parts of the jelly roll were similar [37].

3.5. Direct comparison of cycling ageing

From the results above it can be expected that ageing under moderate conditions is similar for both, 18650 and 21700 formats. Fig. 8 shows the result of cycling tests at 1C for an ambient temperature of 25 °C. The capacity decrease for both cell formats agrees very well to a linear fit, as indicated by the high correlation factors $R^2 \geq 0.98$ in all cases. Furthermore, the ageing results are reproducible for both 18650 and 21700 formats with a second cell each. Interestingly, under the tested condition, both cell formats show very similar capacity decrease per cycle (18650: 0.010 ± 0.001% cycle^{-1}, 21700: 0.010 ± 0.001% cycle^{-1}). This is also consistent with the similarities in the voltage curves in Fig. 1 and with the very similar heating behaviour for discharging at 1C in Fig. 2c.

The similar ageing behaviour under moderate cycling conditions shows that the cell design has a negligible influence under the tested conditions and the main ageing mechanism is clearly dominated by degradation of the materials and electrodes which are the same in both cases.

These results with graphite anodes can be compared to some extend with recent results on SiO–C anodes by Reynier et al. [12]. The authors compared pouch cells with 21700 cells with the same chemistry and also found a similar ageing behaviour [12]. However, in their study, the capacity retention for pouch cells is stronger by ~3% after 300 cycles compared to the 21700 cells [12]. One reason might be higher pressure in the cylindrical format compared to the pouch cell.

We expect that calendar ageing could also be similar for both cylindrical cell formats, provided all used materials and electrodes are the same. We expect an increasing deviation of the ageing behaviour of both cell formats for C-rates above 1C. For example, due to their stronger heating during current flow for high C-rates, it is likely that the ageing rate is slower for 21700 cells at low ambient temperatures due to less susceptibility to Li deposition.

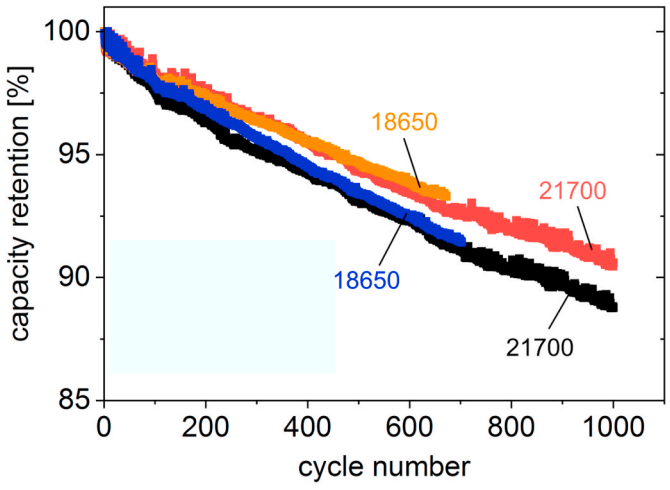

Fig. 8. Direct comparison of capacity retention for cycling at 1C for an ambient temperature of 25 °C.

4. Conclusions

A direct comparison between Li-ion cells in the classic 18650 format and the new 21700 format is made for the first time using the same electrodes, separators, and electrolyte. We showed that the cells are built reproducibly on pilot-scale, with similar deviations between cells like in commercial mass produced cells.

The main differences and similarities between both cell formats are:

1) Charge and discharge voltages curves coincide at low C-rates (0.1C–0.5C) for both formats. For higher C-rates, the polarization gets larger for the 18650 format, leading to deviations in the voltage curves between both formats. Reasons are the lower cell resistance and the stronger heating of the 21700 cells due to current flow.
2) Discharge capacities and energies are higher by ~51% for 21700 in the range of 0.5C–3.75C. This is in agreement with evaluations of CT images and with electrode areas from calculations of the Archimedean spiral's arc length. Comparison of two CT image evaluation methods showed that the jelly roll digitalization method is more accurate and more time consuming compared to evaluation of line-scans.
3) Specific energy and energy density increases by ~6% for the 21700 format for the investigated cells. In our previous estimation with commercial cells the increase of energy density was ~2% [7], which is in the same order of magnitude but shows some potential for optimization.
4) Extensions from the expected 21.0 mm diameter as found in commercial 21700 cells, lead to a fraction of an additional winding and therefore capacity per cell. Stronger extension of the cell diameter can lead to other formats such as 25700 or 30700, which have higher capacities and better energy densities.
5) The electrode curvature decreases with the periodic winding distance d_{ascs} and the winding number and is similar for both cell formats. The electrode curvature leads most likely to compressive stress for electrode coatings facing towards the cell core, especially in the inner windings.
6) The capacity fade as a function of cycles is linear and very similar for both cell formats at a rate of 1C and an ambient temperature of 25 °C.

The presented investigations give valuable insights into differences and similarities between the classic 18650 and the new 21700 format by a direct comparison. The observed trends are most likely similar for other chemistries. Further investigations in this direction are ongoing in our labs.

Declaration of competing interest

The authors declare that they have no known competing financial interests or personal relationships that could have appeared to influence the work reported in this paper.

CRediT authorship contribution statement

Thomas Waldmann: Writing - original draft, Writing - review & editing, Conceptualization, Supervision, Funding acquisition, Project administration, Investigation, Formal analysis, Data curation, Visualization. **Rares-George Scurtu:** Investigation, Visualization. **Karsten Richter:** Investigation, Visualization, Data curation. **Margret Wohlfahrt-Mehrens:** Supervision, Project administration, Funding acquisition.

Acknowledgement

Funding of the project FAB4LIB by the German Federal Ministry of Education and Research (BMBF) under contract n° 03XP0142D and project management by Forschungszentrum Jülich (PTJ) are gratefully acknowledged. Funding of the project DigiBattPro 4.0 (3–4332.62-IPA/69) by the Ministerium für Wirtschaft, Arbeit und Wohnungsbau Baden-Württemberg is gratefully acknowledged. The authors would like to thank the ZSW members A. Fechter for help with building the cylindrical cells as well as M. Kasper, and Dr. M. Bozorgchenani for helpful discussions as well as A. Dautfest (BMZ) for proof-reading of the FAB4LIB part.

References

[1] X. Zhang, Thermal analysis of a cylindrical lithium-ion battery, Electrochim. Acta 56 (2011) 1246–1255, https://doi.org/10.1016/j.electacta.2010.10.054.
[2] D.A.H. McCleary, J.P. Meyers, B. Kim, Three-Dimensional modeling of electrochemical performance and heat generation of spirally and prismatically wound lithium-ion batteries, J. Electrochem. Soc. 160 (2013) A1931–A1943, https://doi.org/10.1149/2.023311jes.
[3] M. Guo, R.E. White, Mathematical model for a spirally-wound lithium-ion cell, J. Power Sources 250 (2014) 220–235, https://doi.org/10.1016/j.jpowsour.2013.11.023.
[4] T. Waldmann, S. Gorse, T. Samtleben, G. Schneider, V. Knoblauch, M. Wohlfahrt-Mehrens, A mechanical aging mechanism in lithium-ion batteries, J. Electrochem. Soc. 161 (2014) A1742–A1747, https://doi.org/10.1149/2.1001410jes.
[5] E.W. Weisstein, From MathWorld–A Wolfram Web resource, Archimedes' spiral, http://mathworld.wolfram.com/ArchimedesSpiral.html, 25th February 2020," n. d.
[6] D. Aurbach, B. Markovsky, A. Rodkin, M. Cojocaru, E. Levi, H.-J. Kim, An analysis of rechargeable lithium-ion batteries after prolonged cycling, Electrochim. Acta 47 (2002) 1899–1911, https://doi.org/10.1016/S0013-4686(02)00013-0.
[7] J.B. Quinn, T. Waldmann, K. Richter, M. Kasper, M. Wohlfahrt-Mehrens, Energy density of cylindrical Li-ion cells: a comparison of commercial 18650 to the 21700 cells, J. Electrochem. Soc. 165 (2018) A3284–A3291, https://doi.org/10.1149/2.0281814jes.
[8] V. Muenzel, A.F. Hollenkamp, A.I. Bhatt, J. de Hoog, M. Brazil, D.A. Thomas, I. Mareels, A comparative testing study of commercial 18650-format lithium-ion battery cells, J. Electrochem. Soc. 162 (2015) A1592–A1600, https://doi.org/10.1149/2.0721508jes.
[9] P. Ramadass, B. Haran, R. White, B.N. Popov, Capacity fade of Sony 18650 cells cycled at elevated temperatures, J. Power Sources 112 (2002) 614–620, https://doi.org/10.1016/S0378-7753(02)00473-1.
[10] T. Waldmann, M. Wilka, M. Kasper, M. Fleischhammer, M. Wohlfahrt-Mehrens, Temperature dependent ageing mechanisms in Lithium-ion batteries – a Post-Mortem study, J. Power Sources 262 (2014) 129–135, https://doi.org/10.1016/j.jpowsour.2014.03.112.
[11] Lain, Brandon, Kendrick, Design strategies for high power vs. High energy lithium ion cells, Batteries 5 (2019) 64, https://doi.org/10.3390/batteries5040064.
[12] Y. Reynier, C. Vincens, C. Leys, B. Amestoy, E. Mayousse, B. Chavillon, L. Blanc, E. Gutel, W. Porcher, T. Hirose, C. Matsui, Practical implementation of Li doped SiO in high energy density 21700 cell, J. Power Sources 450 (2020) 227699, https://doi.org/10.1016/j.jpowsour.2020.227699.
[13] S. Du, M. Jia, Y. Cheng, Y. Tang, H. Zhang, L. Ai, K. Zhang, Y. Lai, Study on the thermal behaviors of power lithium iron phosphate (LFP) aluminum-laminated battery with different tab configurations, Int. J. Therm. Sci. 89 (2015) 327–336, https://doi.org/10.1016/j.ijthermalsci.2014.11.018.
[14] S. Kosch, A. Rheinfeld, S.V. Erhard, A. Jossen, An extended polarization model to study the influence of current collector geometry of large-format lithium-ion pouch cells, J. Power Sources 342 (2017) 666–676, https://doi.org/10.1016/j.jpowsour.2016.12.110.
[15] K.-J. Lee, K. Smith, A. Pesaran, G.-H. Kim, Three dimensional thermal-, electrical-, and electrochemical-coupled model for cylindrical wound large format lithium-ion batteries, J. Power Sources 241 (2013) 20–32, https://doi.org/10.1016/j.jpowsour.2013.03.007.
[16] A. Samba, N. Omar, H. Gualous, O. Capron, P. Van den Bossche, J. Van Mierlo, Impact of tab location on large format lithium-ion pouch cell based on fully coupled tree-dimensional electrochemical-thermal modeling, Electrochim. Acta 147 (2014) 319–329, https://doi.org/10.1016/j.electacta.2014.08.115.
[17] Y. Ye, L.H. Saw, Y. Shi, K. Somasundaram, A.A.O. Tay, Effect of thermal contact resistances on fast charging of large format lithium ion batteries, Electrochim. Acta 134 (2014) 327–337, https://doi.org/10.1016/j.electacta.2014.04.134.
[18] W. Zhao, G. Luo, C.-Y. Wang, Effect of tab design on large-format Li-ion cell performance, J. Power Sources 257 (2014) 70–79, https://doi.org/10.1016/j.jpowsour.2013.12.146.
[19] L.S. Kremer, A. Hoffmann, T. Danner, S. Hein, B. Prifling, D. Westhoff, C. Dreer, A. Latz, V. Schmidt, M. Wohlfahrt-Mehrens, Manufacturing process for improved ultra-thick cathodes in high-energy lithium-ion batteries, Energy Technol. (2019) 1900167, https://doi.org/10.1002/ente.201900167.
[20] K. Richter, T. Waldmann, M. Kasper, C. Pfeifer, M. Memm, P. Axmann, M. Wohlfahrt-Mehrens, Surface film formation and dissolution in Si/C anodes of Li-ion batteries: a glow discharge optical emission spectroscopy depth profiling study, J. Phys. Chem. C 123 (2019) 18795–18803, https://doi.org/10.1021/acs.jpcc.9b03873.
[21] T. Waldmann, G. Bisle, B.-I. Hogg, S. Stumpp, M.A. Danzer, M. Kasper, P. Axmann, M. Wohlfahrt-Mehrens, Influence of cell design on temperatures and temperature gradients in lithium-ion cells: an in operando study, J. Electrochem. Soc. 162 (2015) A921–A927, https://doi.org/10.1149/2.0561506jes.
[22] T. Grandjean, A. Barai, E. Hosseinzadeh, Y. Guo, A. McGordon, J. Marco, Large format lithium ion pouch cell full thermal characterisation for improved electric vehicle thermal management, J. Power Sources 359 (2017) 215–225, https://doi.org/10.1016/j.jpowsour.2017.05.016.
[23] T. Waldmann, M. Wohlfahrt-Mehrens, In-operando measurement of temperature gradients in cylindrical lithium-ion cells during high-current discharge, ECS Electrochem. Lett. 4 (2015) A1–A3, https://doi.org/10.1149/2.0031501eel.
[24] T. Waldmann, M. Kasper, M. Wohlfahrt-Mehrens, Optimization of charging strategy by prevention of lithium deposition on anodes in high-energy lithium-ion batteries – electrochemical experiments, Electrochim. Acta 178 (2015) 525–532, https://doi.org/10.1016/j.electacta.2015.08.056.
[25] C. Veth, D. Dragicevic, C. Merten, Thermal characterizations of a large-format lithium ion cell focused on high current discharges, J. Power Sources 267 (2014) 760–769, https://doi.org/10.1016/j.jpowsour.2014.05.139.
[26] T. Waldmann, B.-I. Hogg, M. Kasper, S. Grolleau, C.G. Couceiro, K. Trad, B. P. Matadi, M. Wohlfahrt-Mehrens, Interplay of operational parameters on lithium deposition in lithium-ion cells: systematic measurements with reconstructed 3-electrode pouch full cells, J. Electrochem. Soc. 163 (2016) A1232–A1238, https://doi.org/10.1149/2.0591607jes.
[27] K. Persson, V.A. Sethuraman, L.J. Hardwick, Y. Hinuma, Y.S. Meng, A. van der Ven, V. Srinivasan, R. Kostecki, G. Ceder, Lithium diffusion in graphitic carbon, J. Phys. Chem. Lett. 1 (2010) 1176–1180, https://doi.org/10.1021/jz100188d.
[28] S. Gorse, B. Kugler, T. Samtleben, T. Waldmann, M. Wohlfahrt-Mehrens, G. Schneider, V. Knoblauch, An explanation of the ageing mechanism of Li-ion batteries by metallographic and material analysis, Pract. Metallogr. 51 (2014) 829–848, https://doi.org/10.3139/147.110325.
[29] T.C. Bach, S.F. Schuster, E. Fleder, J. Müller, M.J. Brand, H. Lorrmann, A. Jossen, G. Sextl, Nonlinear aging of cylindrical lithium-ion cells linked to heterogeneous compression, J. Energy Storage 5 (2016) 212–223, https://doi.org/10.1016/j.est.2016.01.003.
[30] X. Fleury, M.H. Noh, S. Geniès, P.X. Thivel, C. Lefrou, Y. Bultel, Fast-charging of Lithium Iron Phosphate battery with ohmic-drop compensation method: ageing study, J. Energy Storage 16 (2018) 21–36, https://doi.org/10.1016/j.est.2017.12.015.
[31] A. Pfrang, A. Kersys, A. Kriston, D.U. Sauer, C. Rahe, S. Käbitz, E. Figgemeier, Long-term cycling induced jelly roll deformation in commercial 18650 cells, J. Power Sources 392 (2018) 168–175, https://doi.org/10.1016/j.jpowsour.2018.03.065.
[32] X.-G. Yang, C.-Y. Wang, Understanding the trilemma of fast charging, energy density and cycle life of lithium-ion batteries, J. Power Sources 402 (2018) 489–498, https://doi.org/10.1016/j.jpowsour.2018.09.069.
[33] L.K. Willenberg, P. Dechent, G. Fuchs, D.U. Sauer, E. Figgemeier, High-precision monitoring of volume change of commercial lithium-ion batteries by using strain gauges, Sustainability 12 (2020) 557, https://doi.org/10.3390/su12020557.
[34] J. Lamb, C.J. Orendorff, Evaluation of mechanical abuse techniques in lithium ion batteries, J. Power Sources 247 (2014) 189–196, https://doi.org/10.1016/j.jpowsour.2013.08.066.
[35] M.J. Brand, S.F. Schuster, T. Bach, E. Fleder, M. Stelz, S. Gläser, J. Müller, G. Sextl, A. Jossen, Effects of vibrations and shocks on lithium-ion cells, J. Power Sources 288 (2015) 62–69, https://doi.org/10.1016/j.jpowsour.2015.04.107.
[36] D.P. Finegan, M. Scheel, J.B. Robinson, B. Tjaden, I. Hunt, T.J. Mason, J. Millichamp, M. Di Michiel, G.J. Offer, G. Hinds, D.J.L. Brett, P.R. Shearing, In-operando high-speed tomography of lithium-ion batteries during thermal runaway, Nat. Commun. 6 (2015) 6924, https://doi.org/10.1038/ncomms7924.
[37] A.S. Mussa, G. Lindbergh, M. Klett, P. Gudmundson, P. Svens, R.W. Lindström, Inhomogeneous active layer contact loss in a cycled prismatic lithium-ion cell caused by the jelly-roll curvature, J. Energy Storage 20 (2018) 213–217, https://doi.org/10.1016/j.est.2018.09.012.